THEORETICAL AND APPLIED MECHANICS
Volume 43 (2016) Issue 1, 85–98 DOI: 10.2298/TAM160531005K

MECHANICS OF WEATHERED CLAY-MARL ROCK MASSES ALONG THE RUPTURE SURFACE IN HOMOGENEOUS DRY SLOPES

Srđan Kostić, Iva Guranov, Nebojša Vasović, and Dragoslav Kuzmanović

Abstract. Authors analyze stress-strain distribution within slope using the shear stress reduction technique based on finite element method, which was previously confirmed to provide approximately the same results as the Janbu's corrected limit equilibrium method. Results obtained indicate that the largest vertical displacements occur at the slope base and crest, while central part of the slope is exposed to the largest horizontal displacements. Normal and shear stress show maximum values in the middle part of the slope. It was also determined that separate stress-strain relations could be derived for the exact upper and lower part of the rupture surface.

1. Introduction

Mechanics of materials has an important place in geological engineering, since it provides useful theoretical knowledge for deriving appropriate stress-strain relations in earth materials, which are exposed either to the impact of additional forces (load from different constructions) or due to excavation for different engineering purposes (underground exploitation, tunnel construction, etc.). In particular, soil and rock mechanics are used to determine the state of soil and rock masses in natural intact conditions, and to predict their behavior under the effect of various engineering activities or due to action of extreme natural factors. Final goal of such analyzes is to provide construction design so as to prevent the terrain failure, which could be achieved either by reducing the additional forces, by applying some preventive measures (like retaining walls) or by improving the properties of rocks and soils (including grouting, anchoring, etc.). The choice of these additional measures primarily depends on the terrain properties. Soils general behave as continuum environment, hence one could apply existing theoretical knowledge from theory of elasticity in order to obtain appropriate stress-strain relations. On the other hand,

2010 *Mathematics Subject Classification:* 86A60.
Key words and phrases: slope stability, numerical analysis, stress, displacement, shear strain.

rocks represent a discontinuum, meaning that failure occurs along the existing discontinuities by a rule, so one needs to invoke empirical relations in order to define relevant stress states and deformations. Within present paper, analysis is focused on failure in soil in intact natural conditions, with a final goal to provide a complete picture of stress, displacements and stress-strain relations along the rupture surface.

In general, soil failure occurs when shear stress exceeds the shear strength of the material, which could be explained in a following way. If an initial state in a soil is defined as a hydrostatic state, then any normal stress change towards the failure actually represents a differential stress (i.e. difference between the principal stresses), which indicates that a soil failure occurs due to an increment of shear stress [1]. This means that the main parameters that control the stability of soil are soil cohesion and angle of internal friction.

One should note that soil can behave as brittle or ductile under shearing, in dependence on its composition. Clays and very dense sands exhibit pronounced brittle behavior, while medium dense and loose sands are typically ductile materials. In present paper, we assume that-clay marl deposits represent brittle materials, but we do not analyze the effect of residual parameters on the material behavior and obtained results.

Previous studies on this topic were mainly focused on the stress-strain analysis in relation to the laboratory results [2], *in situ* experimental results [3], or stress-strain relations were examined at a specific location as a case study [4, 5]. Theoretical considerations of the stress states and corresponding deformations in relation to landslides have been rarely conducted [6], primarily since real materials behave in a rather unpredictable way, so any deeper mechanical analysis would invoke complex mathematical approach, with results that are hard to apply in engineering practice. In present paper, analysis of soil mechanics along the rupture surface is conducted numerically, using the previously determined ranges of parameter values. The main idea is to provide a global stress-strain mechanism behind the sliding process in weathered clay-marl deposits, since these rock masses are commonly encountered at the edge of Neogene basins (e.g. in large part of Belgrade). Such analysis is not limited to the specific rock mass (shown in present paper), but it could be used for any other terrain construction, including very complex and heterogeneous geological conditions.

Paper is organized as follows. Applied methods are briefly described in Section 2, while results obtained are given in Section 3, including the provision of input parameters, analysis of stress, displacements and stress-strain relations. Conclusions are given in Section 4, together with suggestions for further research.

2. Applied methods

Analysis of soil mechanics along the rupture surface is conducted for homogeneous dry slope in weathered clay-marl deposits. It is assumed that five parameters predominantly control the slope stability: slope height H, slope angle β, unit mass γ, soil cohesion c and angle of internal friction φ. Range of values for each parameter, given in Table 1, is chosen according to commonly obtained laboratory

results for the samples from weathered Neogene clay-marls in Belgrade [7]. Using appropriate experimental design (Box-Behnken) [8], 41 different combinations of input factors were determined, by varying each examined factor on three levels (minimum, medium and maximum value). Such design setup secures the uniform filling of the examined parameter space, providing in that way a solid ground for the inquiry of the reliable regression model. For each case, appropriate slope stability analysis is conducted using Janbu's corrected limit equilibrium method [9]. According to this method of slices, safety factor against sliding could be obtained using the expression in general form [1]:

$$F_s = f_0 \frac{(\sum c\,b + W\mathrm{tg}\varphi)(1/\cos^2\alpha)/(1+\mathrm{tg}\alpha\mathrm{tg}\varphi/F_0)}{\sum W\mathrm{tg}\alpha},$$

where c and φ denote the shear strength parameters (cohesion and angle of internal friction, respectively), while W, b and α stand for the slice weight, slice width and angle of rupture surface at the base of particular slice. Parameter f_0 denotes the correction factor, which depends on the slide geometry and the strength parameters of the soil, and by which one introduces the effect of inter-slice shear forces, while F_0 is the chosen initial value of safety factor. It should be emphasized that summation is done over all the slices within the examined slope. For each analysis, slope is divided into 25 slices, with maximum iteration of 50 steps and acceptable level of tolerance between the two successive values of F_s equal to 0.005. It should be noted that with Janbu's corrected method one obtains safety factor after several iteration steps, starting from the initial guess of F_0.

It should be emphasized that, in present analysis, Janbu's corrected method is chosen for two main reasons. First of all, this method is commonly used for locating the non-circular rupture surfaces in engineering practice. Secondly, convergence is easier to obtain with Janbu's corrected method in comparison to other methods of slices for non-circular rupture surface. Also, the chosen method tends to give lower values of safety factor, which is on the safe side.

Location of critical rupture surface is determined using the Auto Refine Search technique, which is based on iterative search for the critical rupture surface, by gradually narrowing the part of the slope in each iteration where the minimum safety factor is calculated [9]. In each iteration, slope surface is divided into 10 parts, with 10 sliding circles per division. Location of critical rupture surface is determined after 10 iterations, with half of divisions used in every successive iteration.

Results of Janbu's stability analyzes are further corroborated by applying shear strength reduction (SSR) technique based on the finite element method [10]. In this case, factor of safety is obtained by gradually weakening the soil until failure is reached. Numerically, the failure occurs when it is no longer possible to obtain a converged solution [11]. Boundary conditions are such that no displacement is allowed at the left, right and bottom boundary of the model, while movements along surface of the model (slope surface and terrain surface above the slope) are not restricted. In order to exclude the possible effect of boundary conditions on the final result, one has to assume a large enough model, with bottom boundary several

times larger than the slope height. If not, stability of the examined slope could be overestimated, since the potential deeper rupture surfaces with smaller values of F_s would be excluded from the analysis. It should be emphasized that, for each analysis, model of slope is uniformly discretized with 3000 six-noded triangles. Also, for each analysis, authors estimated initial value of 1 for F_s, with the step size equal to 0.01 in each iteration.

One should note that the main advantage of using the SSR technique over the traditional methods of slices lies in its ability to provide the actual displacements along the determined rupture surface. However, the slope stability analysis based on finite element method could be conducted only numerically, which makes it slightly inconvenient for engineering practice.

Authors emphasize that nomenclature used in present paper is adjusted to valid recommendations of UNESCO Working Party for World Landslide Inventory [12].

3. Results

3.1. Slope stability analysis. Results of slope stability analyzes using Janbu's corrected limit equilibrium method and shear strength reduction technique (SSR) are given in Table 2, for 41 different combinations of the influential parameters, determined using the Box-Benhken statistical design, so as to uniformly fill the observed parameter space. This comparison of traditional Janbu corrected method and SSR technique is an obligatory step, since there is no direct evidence of the equal results obtained when applying both of these methods for solving the same problem.

As one could see in Table 2, limit equilibrium method and shear strength reduction (SSR) technique provide approximately the same results, so one could continue with further analysis using only the SSR method, since it enables stress-strain analysis of slope in a critical state. One should note that SSR method is applied under the following assumptions:

(1) assumed peak tensile strength is equal to cohesion;
(2) peak and residual shear strength parameters are equal;
(3) Poisson ration is assumed to take the value $\nu = 0.4$;
(4) Young's modulus is assumed constant, $E = 50\,\text{MPa}$.

TABLE 1. Examined range of values for the chosen input parameters for weathered clay-marl rock masses.

Input parameters	minimum value	maximum value
H (m)	3	25
β (°)	10	25
γ (kN/m^3)	16	23
c (kPa)	9	90
φ (°)	13	22

Further analysis of stress, displacements and stress-strain relations is conducted for the case with the smallest value of the safety factor ($F_s = 1.133$, for the case

TABLE 2. Input data for slope stability analyzes determined by experimental design and corresponding calculated values of F_s using Janbu's method and SSR technique.

Case No.	H (m)	$\beta(^\circ)$	γ (kN/m^3)	c (kPa)	$\varphi(^\circ)$	F_s (Janbu)	F_s (SSR)
1	3	10	19.5	49.5	17.5	8.483	8.73
2	25	10	19.5	49.5	17.5	3.1	3.14
3	3	25	19.5	49.5	17.5	6.78	6.56
4	25	25	19.5	49.5	17.5	1.717	1.72
5	14	17.5	16	9	17.5	1.584	1.59
6	14	17.5	23	9	17.5	1.46	1.46
7	14	17.5	16	90	17.5	4.32	4.37
8	14	17.5	23	90	17.5	3.46	3.52
9	14	10	19.5	49.5	13	3.147	3.24
10	14	25	19.5	49.5	13	2.05	2.02
11	14	10	19.5	49.5	22	4.43	4.51
12	14	25	19.5	49.5	22	2.591	2.6
13	3	17.5	16	49.5	17.5	8.47	8.45
14	25	17.5	16	49.5	17.5	2.307	2.34
15	3	17.5	23	49.5	17.5	6.437	6.5
16	25	17.5	23	49.5	17.5	1.99	2.03
17	14	17.5	19.5	9	13	1.195	1.2
18	14	17.5	19.5	90	13	3.405	3.44
19	14	17.5	19.5	9	22	1.839	1.84
20	14	17.5	19.5	90	22	4.231	4.32
21	14	10	16	49.5	17.5	4.09	4.2
22	22	25	16	49.5	17.5	2.608	2.59
23	23	10	23	49.5	17.5	3.56	3.63
24	24	25	23	49.5	17.5	2.11	2.12
25	25	17.5	19.5	9	17.5	2.54	2.65
26	26	17.5	19.5	9	17.5	1.35	1.34
27	27	17.5	19.5	90	17.5	11.65	11.53
28	28	17.5	19.5	90	17.5	2.775	2.82
29	29	17.5	16	49.5	13	2.65	2.7
30	30	17.5	23	49.5	13	2.167	2.21
31	31	17.5	16	49.5	22	3.44	3.5
32	32	17.5	23	49.5	22	2.917	2.97
33	33	17.5	19.5	49.5	13	6.78	6.77
34	34	17.5	19.5	49.5	13	1.777	1.8
35	35	17.5	19.5	49.5	22	7.767	7.86
36	36	17.5	19.5	49.5	22	2.486	2.52
37	37	10	19.5	9	17.5	2.414	2.4
38	38	25	19.5	9	17.5	1.133	1.14
39	39	10	19.5	90	17.5	4.925	5.07
40	40	25	19.5	90	17.5	3.37	3.32
41	41	17.5	19.5	49.5	17.5	2.75	2.8

No. 38). Since relevant results are obtained only for the slope at the verge of stability ($F_s \approx 1$), one can slightly change the values of unit mass and shear strength parameters in order to reduce the slope stability. In order to do so, one should firstly establish reliable correlation among the influential parameters and the slope safety factor (Fig. 1).

As it could be seen from Figure 1, increase of cohesion and friction angle increases the slope stability, while the increase of slope height and angle, and unit mass leads to a decrease of the slope safety factor. For the case No. 38 with the smallest value of safety factor from Table 2, value of friction angle is being reduced, while value of unit mass is being increased, until critical value of slope safety factor ($F_s \approx 1$) is obtained ($\varphi = 15°$, $\gamma = 21\,\mathrm{kN/m^3} \Rightarrow F_{s_{\mathrm{Janbu}}} = 0.988$, $F_{s_{\mathrm{SSR}}} = 1$).

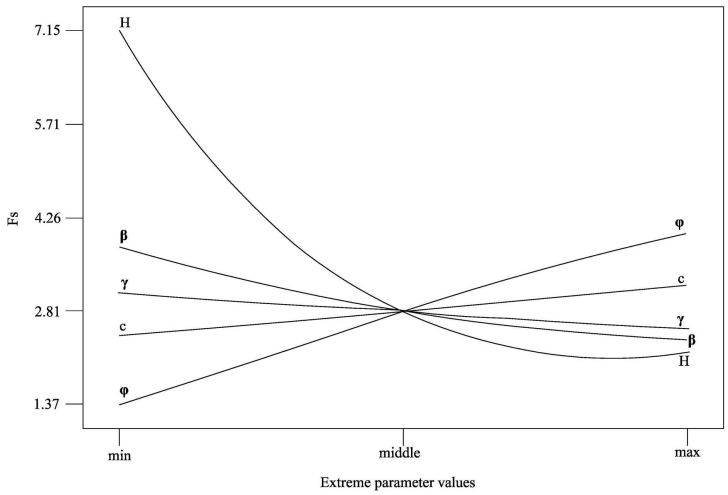

FIGURE 1. Individual effect of examined influential factors on slope stability. While a single parameter is varied, others are being held constant at their average values (for specific values please refer to Table 1).

3.2. Analysis of displacements. Regarding the recorded displacements, both vertical and horizontal, one could notice from Fig. 2 the pronounced subsidence at the slope crest, and increased uplift at the slope base. This corresponds well to the expected mechanism of sliding due to gravitational effect.

As it could be seen from the diagram of vertical displacements along the slope (Fig. 2b), there are two points on the slope with pronounced deformation:

(1) lower part of the slope, i.e. slope base exhibits vertical uplift, due to the pressure of the depleted mass from the upper part;
(2) upper part of the slope, i.e. slope crest exhibits vertical subsidence, due to downward movement of the depleted mass under the gravitational effect.

Regarding the horizontal displacements (Fig. 3), one can observe that the middle part of the slope is exposed to the largest deformation, due to the downward

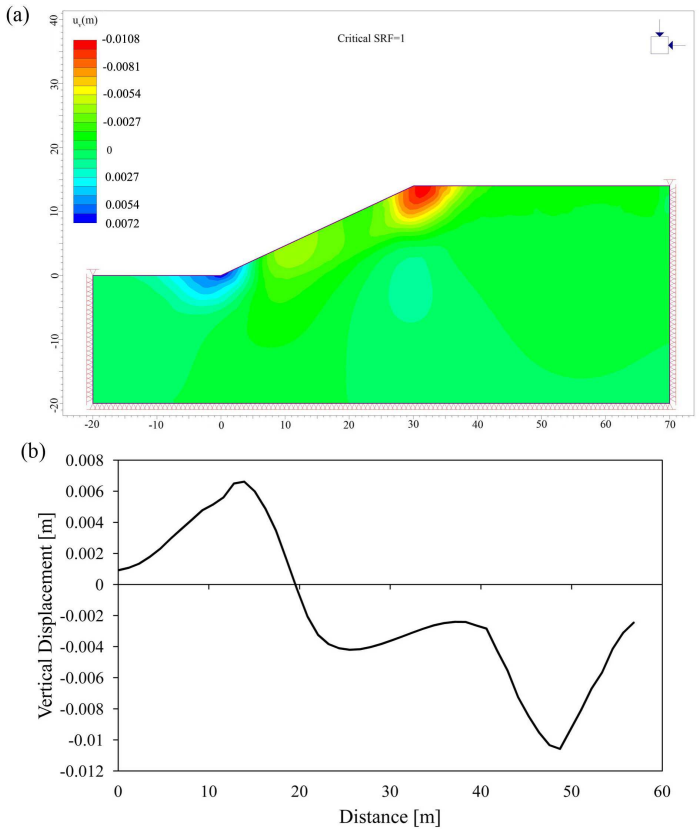

FIGURE 2. Vertical displacements determined by SSR technique: (a) Distribution of vertical displacements within the analyzed slope; (b) Diagram of vertical displacements along the slope surface. Acronym SRF denotes the Strength Reduction Factor, i.e. safety factor determined by Shear Stress Reduction technique.

movements of the depleted mass, which cause pronounced vertical displacements at the slope base and crest, and significant horizontal displacements in the central part of the slope.

Distribution of maximum shear strain clearly indicates the location of the surface of rupture (Fig. 4). One should notice that, for a more comprehensible view, maximum shear strain distribution is shown for the case SRF = 1.01. In this case, maximum shear strain is defined in the following way:

$$\varepsilon_{xy\,\max} = \frac{\varepsilon_1 - \varepsilon_2}{2} = \frac{1}{2}\left(\frac{\varepsilon_x + \varepsilon_y}{2} + \sqrt{\left(\frac{\varepsilon_x - \varepsilon_y}{2}\right)^2 + \left(\frac{\gamma_{xy}}{2}\right)^2}\right) - \frac{1}{2}\left(\frac{\varepsilon_x + \varepsilon_y}{2} - \sqrt{\left(\frac{\varepsilon_x - \varepsilon_y}{2}\right)^2 + \left(\frac{\gamma_{xy}}{2}\right)^2}\right)$$

where ε_1 and ε_2 are principal strains, ε_x and ε_y are the normal strains in the x and y directions, respectively, while γ_{xy} represents the engineering shear strain [13].

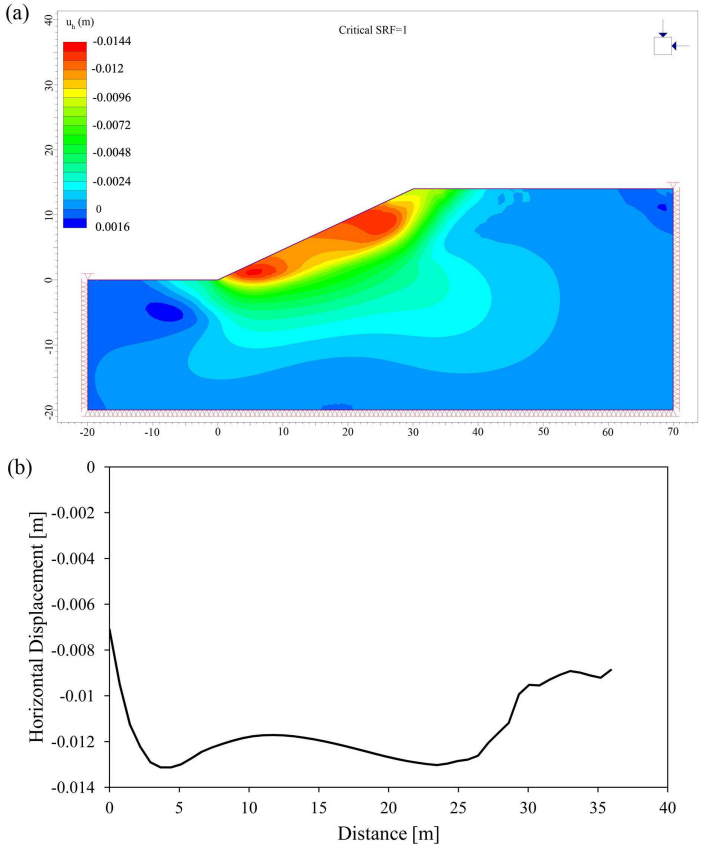

FIGURE 3. Horizontal displacements determined by SSR technique:(a) Distribution of horizontal displacements within the analyzed slope; (b) Diagram of horizontal displacements along the slope surface. Acronym SRF denotes the Strength Reduction Factor, i.e. safety factor determined by Shear Stress Reduction technique.

3.3. Analysis of stress. Regarding the distribution of stress along the rupture surface, results obtained indicate that both normal and shear stress increase along the surface (Fig. 5). This is expected since it was assumed that failure occurs

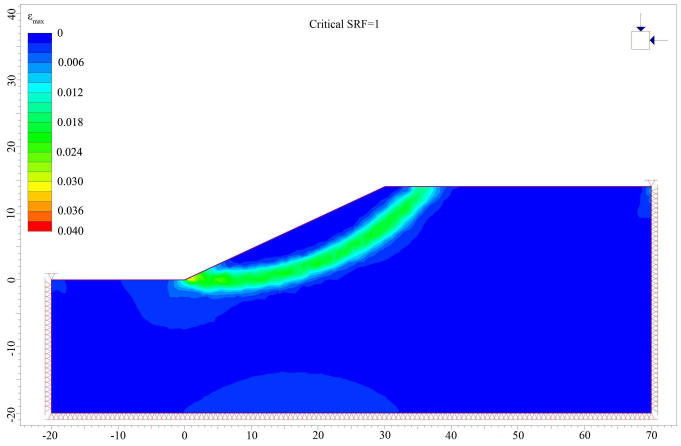

FIGURE 4. Distribution of maximum shear strain within the analyzed slope, clearly indicating the position of the rupture surface (for F_s=1). Acronym SRF denotes the Strength Reduction Factor, i.e. safety factor determined by Shear Stress Reduction technique.

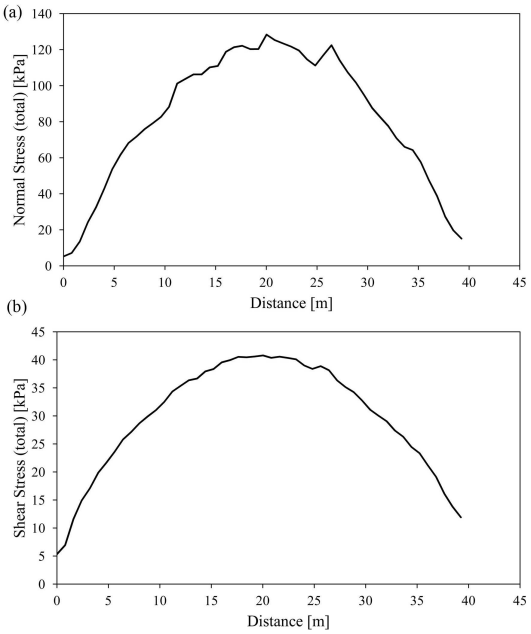

FIGURE 5. Diagram of normal stress (a) and shear stress (b) along the surface of rupture.

according to Mohr–Coulomb criterion:

$$\tau = c + \sigma \operatorname{tg}\varphi$$

where σ and τ are normal and shear stress, respectively, and c and φ denote cohesion and angle of internal friction, respectively. Since, in present analysis, cohesion and friction angle are assumed to have constant values, it follows that normal and shear stress are directly proportional, which explains the same trend of their change along the rupture surface. As for the relation between the stress and material strength, in the examined case, when $F_s \approx 1$, shear stress reaches the shear strength along the rupture surface (Fig. 6).

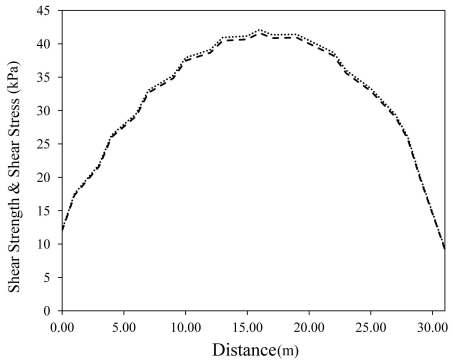

FIGURE 6. Diagrams of shear stress (dashed line) and shear strength (dotted line) along the surface of rupture.

3.4. Stress-strain relations. In general, stress-strain relations are given rheological models, i.e. they describe temporal evolution of stress and corresponding strain for a specific type of material. In present analysis, stress-strain relations are examined along the rupture surface at the moment of failure. Thereby, authors define relation between the shear stress (which, actually, controls the failure) and vertical and horizontal displacements along the rupture surface, including the resulting maximum shear strain.

Obtained results indicate rather interesting phenomenon: stress-strain relations in the exact upper and lower part of the rupture surface could be perfectly described by spline function as a combination of the two higher-order polynomial functions (Figs. 7 and 8):

$$u_{vl} = \begin{cases} -5\cdot 10^{-8}\cdot \tau^4 + 4\cdot 10^{-6}\cdot \tau^3 - 0,0001\cdot \tau^2 + 0.0009\cdot \tau - 0.0095 & \ell \leqslant d/2 \\ -4\cdot 10^{-8}\cdot \tau^4 + 5\cdot 10^{-6}\cdot \tau^3 - 0,0002\cdot \tau^2 + 0.0029\cdot \tau - 0.0062 & \ell > d/2 \end{cases}$$

$$u_{hl} = \begin{cases} -3\cdot 10^{-8}\cdot \tau^4 + 2\cdot 10^{-6}\cdot \tau^3 - 5\cdot 10^{-5}\cdot \tau^2 + 0.0004\cdot \tau - 0.006 & \ell \leqslant d/2 \\ 2\cdot 10^{-8}\cdot \tau^4 - 2\cdot 10^{-6}\cdot \tau^3 + 6\cdot 10^{-5}\cdot \tau^2 + 0.0004\cdot \tau - 0.0083 & \ell > d/2 \end{cases}$$

$$\varepsilon_\ell = \begin{cases} -2\cdot 10^{-7}\cdot \tau^3 + 3\cdot 10^{-5}\cdot \tau^2 - 0.0012\cdot \tau + 0.0181 & \ell \leqslant d/2 \\ 3\cdot 10^{-8}\cdot \tau^4 - 3\cdot 10^{-6}\cdot \tau^3 + 0.0001\cdot \tau^2 - 0.003\cdot \tau - 0.0285 & \ell > d/2 \end{cases}$$

Variables u_{vl} and u_{hl} stand for the vertical and horizontal displacement along the rupture surface, while l denotes part of the rupture surface that is described by the corresponding polynomial regression ($\ell \leqslant d/2$ denotes the lower part of the rupture surface, $\ell > d/2$ stands for the upper part of the rupture surface). Variables τ and ε represent total shear stress and maximum shear strain along the rupture surface.

4. Conclusion

In present paper authors perform systematic analysis of stress-strain distribution within a slope at the verge of stability, composed of weathered Neogene clay-marls deposits. It is assumed that slope stability is controlled by the variation of five main parameters: slope height and angle, unit mass, cohesion and angle of internal friction. Analysis is performed for the simple case of homogeneous slope without the effect of pore water pressure. Research is conducted using the

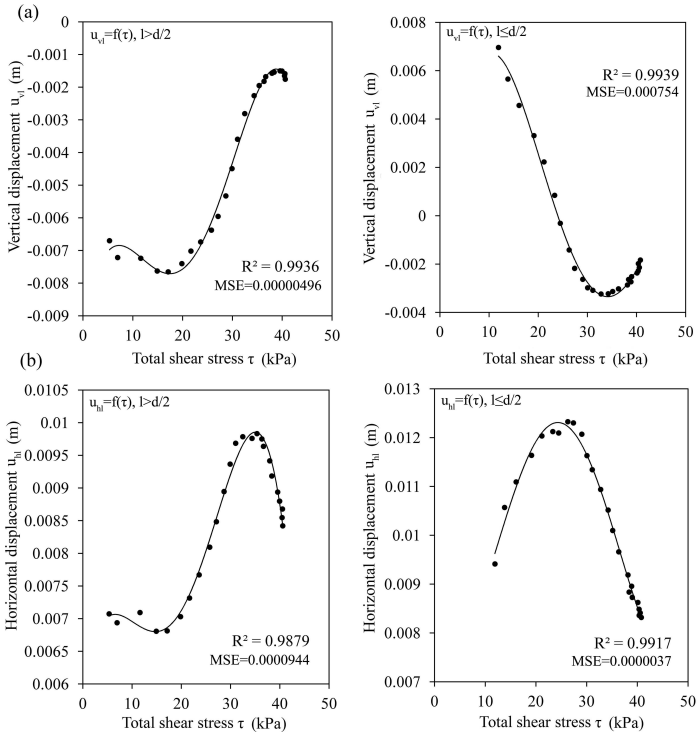

FIGURE 7. Stress-strain relation along the rupture surface: (a) total shear stress vs. vertical displacement; (b) total shear stress vs. horizontal displacement. Polynomial regressions on the left side are given for the upper part of the rupture surface, while right side shows polynomial regressions for the lower part of the rupture surface. For simplicity, regression was performed for absolute values of horizontal displacements.

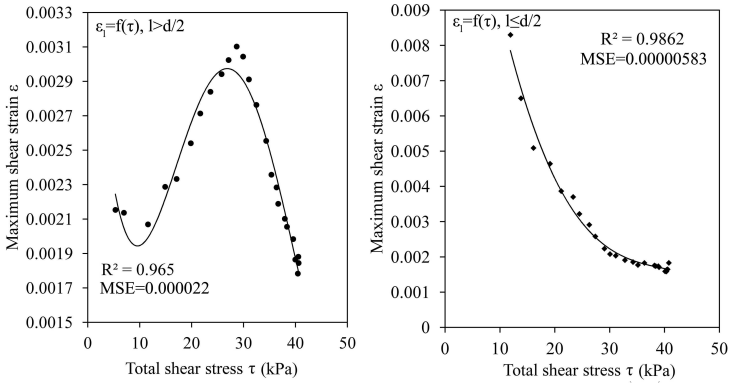

FIGURE 8. Diagrams of total shear stress vs. maximum shear strain along the surface of rupture. Polynomial regression on the left side is given for the upper part of the rupture surface, while right side shows polynomial regression for the lower part of the rupture surface.

shear strength reduction technique based on the finite element method in *Phase*® *RocScience*, for which it was previously determined to provide approximately the same results as the application of Janbu's corrected limit equilibrium method.

Results obtained indicate that the largest vertical displacements occur at the slope base and crest, while the largest horizontal displacements are determined in the central part of the slope. Such strain distribution is expected, since depleted mass is moving under the effect of gravity (i.e. its own weight). Normal and shear stress have the highest values at the middle part of the rupture surface. As for the relation between the shear strain and shear stress, results of the performed research imply that maximum shear strain is observed in the middle of the upper part of the slope, and at the slope base. Concerning this, one could conclude that the value of maximum shear strain in the middle part of slope is controlled by the horizontal deformation, while the maximum shear strain at the slope base is governed by vertical deformation.

As for the determined stress-strain relations, it was found that separate expressions could be given for the exact upper and lower part of the sliding surface, using polynomial regression with high statistical reliability. Derived expressions could be used for prediction of stress-strain distribution within the slope in Neogene clay-marl deposits at the verge of stability. Also, one could adopt presented approach for developing separate stress-strain expressions for slopes composed of other geological units.

Presented research represents only the starting phase of stress-strain analysis of a slope subjected to sliding. Further research should include the effect of pore water on stress-strain distribution in heterogeneous geological conditions, providing, in that way, a complete picture of the state of stress and strain for instability-prone slopes.

Acknowledgments. Presented work was partly supported by the Ministry of Education, Science and Technological Development of the Republic of Serbia (Contract No. 37005).

References

1. M. Maksimović, *Soil Mechanics*, AGM book Belgrade, (2008) (in Serbian).
2. K. Sasahara, N. Sakai, *Development of shear deformation due to the increase of pore pressure in a sandy model slope during rainfall*, Eng. Geol. **170** (2014), 43–51.
3. F. Casini, C. Jommi, S. Springman, *A laboratory investigation on an undisturbed silty sand from a slope prone to landsliding*, Granul. Matter **12** (2010), 303–316.
4. F. Darve, F. Laouafa, *Instabilities in granular materials and application to landslides*, Mech. Cohesive-Frictional Mater. **5** (2000), 627–652.
5. A. C. Trandafir, Z. A. Amini, *Yielding mechanism of shallow mass movements in completely decomposed Norwood Tuff: the Zigzag Sign landslide, Utah*, Environ. Geol. **57** (2009), 1443–1451.
6. N. Thompson, M. R. Bennett, N. Petford, *Analyses on granular mass movement mechanics and deformation with distinct element numerical modeling: implications for large-scale rock and debris avalanches*, Acta Geotechnica **4** (2009), 233–247.
7. S. Kostić, N. Vasović, D. Jevremović, *Stability of earth slopes under the effect of main environmental properties of weathered clay-marl deposits in Belgrade (Serbia)*, Environ. Earth Sci. **75** (2016), 1–10.
8. S. N. Deming, S. L. Morgan, *Experimental design: a chemometric approach*, Elsevier Amsterdam, (1996).
9. Rocscience Inc. Phase^2 Version 8.0. 2D Limit Equilibrium Slope Stability Analysis, www.rocscience.com, Toronto, Ontario, Canada, 2002.
10. Rocscience Inc. Slide Version 5.0. 2D Elasto-Plastic Finite Element Stress Analysis for underground or surface excavations, www.rocscience.com, Toronto, Ontario, Canada, 2002.
11. E. M. Dawson, W. H. Roth, A. Drescher, *Slope stability analysis by strength reduction*, Geotechnique **49** (1999), 835–840.
12. WP/WLI: International Geotechnical Societies' UNESCO Working Party on World Landslide Inventory (Chairman: D.M.Cruden) *Multilingual Landslide Glossary*, Bitech, Richmond, British Columbia (1993), 1–59.
13. B. Budiansky, *On the elastic moduli of some heterogeneous materials*, J. Mech. Phys. Solids **13** (1965), 223–227.

МЕХАНИЧКО ПОНАШАЊЕ РАСПАДНУТИХ ГЛИНОВИТО-ЛАПОРОВИТИХ СТЕНСКИХ МАСА ДУЖ КЛИЗНЕ ПОВРШИ У ХОМОГЕНИМСУВИМ КОСИНАМА

Резиме. Аутори врше анализу напона и деформација у нестабилној косини коришћењем технике редукције смичућег напона, која се заснива на методи коначних елемената. У раду је потврђено да ова техника даје приближо исте резултате као и Јанбуова коригована метода граничне равнотеже. Резултати анализе указују на појаву највећих вертикалних померања у ножици и врху косине, док је средишњи део косине изложен највећим хоризонталним померањима. Изведеним истраживањем је утврђено да нормални и смичући напони достижу највеће вредности у средишњем делу косине. Такође је показано да критична клизна површ може да се подели на једнака два дела, за које важе статистички значајне везе напона и деформација.

Institute for Development of Water Resources "Jaroslav Černi"
Belgrade
Serbia
srdjan.kostic@jcerni.co.rs

University of Belgrade
Faculty of Mechanical Engineering
Belgrade
Serbia
iva.guranov@gmail.com

University of Belgrade
Faculty of Mining and Geology
Belgrade
Serbia
nebojsa.vasovic@rgf.bg.ac.rs

University of Belgrade
Faculty of Transport and Traffic Engineering
Belgrade
Serbia
d.kuzmanovic@sf.bg.ac.rs

(Received 31.05.2016)
(Revised 17.06.2016)
(Available online 24.06.2016)